Soft Matter

Phase diagrams of mixtures of dipolar rods and discs

Journal:	*Soft Matter*
Manuscript ID	SM-ART-06-2018-001225.R1
Article Type:	Paper
Date Submitted by the Author:	28-Aug-2018
Complete List of Authors:	Maloney, Ryan; North Carolina State University, Chemical and Biomolecular Engineering Hall, Carol; North Carolina State University, Chemical and Bimolecular Engineering

Soft Matter

ARTICLE

Phase diagrams of mixtures of dipolar rods and discs

Ryan C. Maloney[a] and Carol K. Hall*[a]

Received 00th January 20xx,
Accepted 00th January 20xx

DOI: 10.1039/x0xx00000x

www.rsc.org/

Self-assembly of binary mixtures that contain anisotropic, interacting colloidal particles have been proposed as a way to create new, multi-functional materials. We simulate binary mixtures of dipolar rods and dipolar discs in two-dimensions using discontinuous molecular dynamics to determine how the assembled structures of these mixtures differs from those seen in single component systems. Two different binary mixtures are investigated: a mixture of an equal number of dipolar rods and dipolar discs ("equal number"), and a mixture where the area fraction of dipolar rods is equal to the area fraction of dipolar discs ("equal area"). Phase boundaries between fluid, string-fluid, and "gel" phases are calculated and compared to the phase boundaries of the pure components. Looking deeper at the underlying structure of the mixture reveals complex interplay between the rods and discs and the formation of states where the two components are in different phases. The mixtures exhibit phases where both rods and discs are in the fluid phase, where rods form a string fluid while discs remain in the fluid phase, a rod string-fluid coexisting with a disc string-fluid, a "gel" that consists primarily of rods while the discs form either a fluid or string-fluid phase, and a "gel" that contains both rods and discs. Our results give insight into the general assembly pathway of binary mixtures, and how complex aggregates can be created by varying the mixture composition, strength of interaction between the two components, and the temperature. By manipulating the properties of one of the components it should be possible to fabricate bifunctional, thermally responsive self-assembled materials.

Introduction

Colloid self-assembly can, in principle, be precisely controlled, resulting in a variety of structures that have proposed for applications in biotechnology,[1-3] photonics,[4-7] and electronic devices.[8-10] The wide variety of colloidal particles that can be created yields systems with unique rheological, viscoelastic, and gelation behavior. Concentrated colloidal gels have been used as inks in 3-D printing to create precise periodic structures.[11] Long chains of colloidal particles have been used as nanowires for light-emitting diodes,[12] and chemical/biological sensors.[13] Ferromagnetic nanoparticles have been used to create artificial cilia.[14] New fabrication techniques allow for precise control over the size, permeability, and elasticity of colloidal capsules that can be used for drug delivery.[15] The wide array of potential applications drives the desire to study systems of ever-increasing complexity.

Colloids that contain one or more sources of anisotropy, either through shape, surface coating, or internal charge distribution, are of interest because the asymmetric interaction between particles gives rise to complex behavior. One of the most extensively studied anisotropic colloids is the dipolar colloidal sphere. Experiments,[16-18] analytical theories,[19-23] and computer simulations[24-30] have been used to evaluate the self-assembly behavior of these particles. Dipolar spheres in 2-D have been shown to assemble into chains, gels, rings, and branched structures at low volume fraction in addition to forming crystalline phases at high volume fraction.[31] The specific phase that forms, and its stability, are related to the concentration of particles and the temperature. More complex 2-D structures can be achieved through the application of external magnetic or electric fields. Application of a homogenous field in one direction causes dipolar spheres to align into chains of finite length.[32] Dipolar spheres in a rotating field assemble in layers rotating with either synchronous or asynchronous behavior.[33]

Rod-shaped particles have also been widely investigated due to their tendency to form nematic and smectic phases that can be used for display devices. Monte Carlo simulations with Gibbs-Duhem integration found that the phases formed by rod-shaped colloids depend on their aspect ratio and concentration.[34] Additionally, rod-shaped particles can be fabricated with patchy surfaces or asymmetric charge distribution, thereby adding an additional source of anisotropy to gain further control and complexity over the self-assembled structures. External electric fields have been used to induce a dipole in rods that causes them to assemble into rings[35] or chains aligned in a head-to-tail or side-by-side orientation in 2-D[36,37] depending on the fabrication techniques and the materials used in their preparation. Gold nanorods coated with cetyl trimethyl ammonium bromide on the sides and polystyrene on the ends have been assembled into both head-to-tail and side-side oriented chains, rafts, and spherical structures, depending on solvent quality.[38] Rods with permanent dipoles oriented in the direction of the short axis

[a] Department of Chemical & Biomolecular Engineering, North Carolina State University, Raleigh, NC 27695, USA. E-mail: hall@ncsu.edu

Electronic Supplementary Information (ESI) available: [Discontinuous potential analysis and additional simulation cell images]. See DOI: 10.1039/x0xx00000x

can assemble into ribbons and rings.[39] To the best of our knowledge, the fabrication of rods with a permanent dipole oriented in the direction of the long axis has yet to be achieved, but with the rapid advancement in fabrication techniques in recent years, it is only a matter of time before such particles are created. In the meantime, discontinuous molecular dynamics simulations of 2-D rods with an extended dipole have shown that the charge separation on the dipole moment plays a key role in determining if rods align with predominately head-to-tail or side-side orientation.[40]

In addition to creating colloidal particles with new anisotropy, studies have been done on mixing particles to create new materials. Monte Carlo simulations of binary mixtures of colloidal spheres of many different diameters and interaction energies have shown that these mixtures always form a percolated network at a lower density than that required for percolation of either pure system.[41] Experiments on mixtures of oppositely-charged spherical colloids show that they form crystalline arrays when the charge is low, but irreversibly aggregate into fractal structures when the charge is high.[42, 43] The aggregation of oppositely charged colloids can be directed by using an AC electric field to form chains in two dimensions.[44] Discontinuous molecular dynamics (DMD) simulations of mixtures of dipolar colloidal spheres have shown that the spheres assemble into bicontinuous gels.[45] Mixtures of rod-shaped liquid crystals and spherical colloids have been of particular interest. Monte Carlo simulations[46] and experiments[47] have shown that mixtures of hard rods and hard spheres undergo entropically-driven phase separation into lamellar, columnar, and miscible phases, depending on the overall colloid concentration and the relative concentrations and sizes of the rods and spheres. Theoretical predictions[48] from four decades ago which predicted that large spherical magnetic particles suspended in nematic liquid crystals could produce macroscopic ferromagnetic phases have recently been experimentally realized.[49] Molecular dynamics (MD) simulations have been used to expand upon these results, focusing on the organization and dynamics of magnetic spheres of similar or smaller size than the width of the rods in the liquid crystal.[50-52]

In this paper, we present results from DMD simulations of two-dimensional mixtures of dipolar rods and dipolar discs. Two mixtures are simulated: one with an equal number of rods and discs ("equal number mixture"), and the other where the areas occupied by rods and discs are equal ("equal area mixture"). The dipolar rods have a length to width ratio of 4:1, which is lower than the aspect ratio at which rods form nematic and smectic phases in two dimensions.[53] By limiting the possibility of forming liquid crystalline phases, we focus our attention on those aspects of the phase behavior due to the dipolar interactions between rods, between discs, and between rods and discs. We perform simulated annealing simulations, which involves running fixed area fraction simulations at a high temperature and then lowering the temperature in discrete steps, allowing the system to equilibrate at each temperature. We compute extent of polymerization and percolation probability to determine when the mixtures transition from a fluid to string-fluid and string-fluid to percolated network respectively. The string-fluid to percolated network transition is of particular interest because percolation is a necessary criterion for gelation. Additionally, we compare the phase transitions found in the mixtures to the phase transitions found in the constituent single component systems.

Highlights of our results include the following. Phase diagrams in the area fraction versus temperature plane were calculated for equal number and equal area mixtures of dipolar rods and discs, with particular focus on the fluid, string-fluid, and "gel" phases. For both mixtures at high temperature, rods preferentially form clusters with other rods creating a rod string fluid, while the discs remain in the fluid phase. After the formation of the rod string fluid, the two mixtures behave differently as the temperature is lowered. In the equal number mixture, the onset of gelation is characterized by formation of a rod "gel" that encompasses nearly all the rods in the system and very few discs. Lowering the temperature results in a coarsening of the rod "gel" through side-by-side rod interactions, with the discs beginning to form small clusters in the voids of the rod network. Finally, at the lowest temperatures simulated, a rod and disc "gel" forms that is characterized by a large network of rods with discrete clusters of discs. In the equal area mixture, the onset of gelation is characterized by the formation of a rod "gel" that contains nearly all the rods in the system, but also many discs. Lowering the temperature results in the formation of small clusters of discs in the voids of the rod network, but the rod network does not coarsen as in the equal number mixture. Finally, at the lowest temperatures simulated, a rod and disc "gel" forms that is characterized by discrete clusters of rods that get connected to one another through clusters of discs. The rod and disc "gel" of both mixtures has a large number of rod-rod and disc-disc interactions, but a relatively small number of rod-disc interactions. The phase transitions found in the equal area mixture closely match to the phase transitions exhibited by pure dipolar discs, while the phase transitions in the equal number mixture are more like those for pure dipolar rods.

Model

We model each dipolar disc as a hard disc with diameter σ containing two oppositely-charged small discs of diameter 0.3σ that are separated by a distance of 0.6σ, as shown in Figure 1(a). The dipolar rods are modeled as spherocylinders with seven overlapping hard discs of diameter σ separated from their nearest neighbors by 0.5σ. The seven overlapping hard discs create a rod with a 4:1 aspect ratio, which is comparable to the aspect ratio of silica-coated gold nanorods created by Wu and

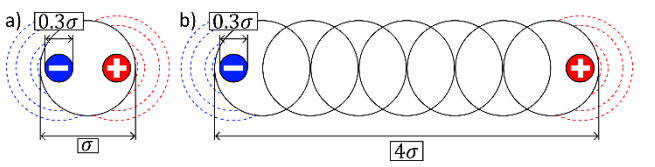

Figure 1: Model of (a) dipolar disc of diameter σ and (b) 4σ:1σ aspect ratio dipolar rod.

Tracy.[54] Two small, oppositely charged discs of diameter 0.3σ are imbedded in the end discs to represent charges on the extended dipole as shown in Figure 1(b). The distance between the two charged discs on the dipolar rods is 3.6σ. The overlapping hard discs on the same chain do not interact with each other, but are bonded to their nearest and next-nearest neighbors using the Bellemans' method.[55, 56] The length of the bond linking neighboring discs varies between $(1+\delta)\sigma 2$, and $(1-\delta)\sigma 2$. The length of the bond linking next-nearest neighboring discs is between $(1+\delta)\sigma$ and $(1-\delta)\sigma$. The Bellemans' constant, δ, defines how tightly the discs that make up the rod are bound to each other and is set equal to 0.02. This value ensures a relatively rigid rod, with the angle between the two end discs and the center disc on a rod greater than or equal to 170 degrees.

The two small discs representing charges of an extended dipole are used to model the dipolar interaction instead of a point dipole. This is done to facilitate the use of the DMD technique, which requires isotropic interactions around each simulated structure. A dipole-dipole interaction potential between point dipoles is not isotropic, and therefore would not be suitable for DMD. We replace the point dipoles with two opposite charges and can then treat each charge as being at the center of an isotropic square well and shoulder potential. The Bellemans' method is then used to maintain the position of the two charges on the dipolar discs and dipolar rods. The small charged discs on a dipolar disc are bonded to each other with a bond length between $(1+\delta)0.6\sigma_1$ and $(1-\delta)0.6\sigma_1$. Each charged disc is also bonded to the main hard disc with bond lengths between $(1+\delta)0.3\sigma_1$ and $(1-\delta)0.3\sigma_1$. The small charged discs on the dipolar rod are bonded to each other with bond lengths of $(1+\delta)3.6\sigma_1$ and $(1-\delta)3.6\sigma_1$, and each charged disc is bonded to the hard disc at the end of the rod that they are closest to with a bond length between $(1+\delta)0.3\sigma_1$ and $(1-\delta)0.3\sigma_1$.

The hard discs of a dipolar disc or rod interact with other colloids through the hard sphere potential (U_{HS}), defined as:

$$U_{HS}(r_1) = \begin{cases} \infty, & if\ r_1 < \sigma \\ 0, & if\ r_1 \geq \sigma \end{cases} \quad (1)$$

where r_1 is the distance between two hard discs. Charged discs on the same colloid do not interact. Charged discs i and j on different colloids interact via an attractive four-step square-well potential if the charges are of opposite sign, or a repulsive four-step square-shoulder potential if the charges have the same sign. The four-step square-well and square-shoulder potentials are defined as:

$$U_{rod-rod}(r_{ij}) = \begin{cases} \infty, & if\ r_2 < \sigma_1 \\ \pm\varepsilon_1, & if\ \sigma_1 \leq r_2 < \sigma_2 \\ \pm\varepsilon_2, & if\ \sigma_2 \leq r_2 < \sigma_3 \\ \pm\varepsilon_3, & if\ \sigma_3 \leq r_2 < \sigma_4 \\ \pm\varepsilon_4, & if\ \sigma_4 \leq r_2 < \sigma_5 \\ 0, & if\ r_2 \geq \sigma_5 \end{cases} \quad (2)$$

$$U_{disc-disc}(r_{ij}) = \begin{cases} \infty, & if\ r_2 < \sigma_1 \\ \pm\varepsilon_5, & if\ \sigma_1 \leq r_2 < \sigma_2 \\ \pm\varepsilon_6, & if\ \sigma_2 \leq r_2 < \sigma_3 \\ \pm\varepsilon_7, & if\ \sigma_3 \leq r_2 < \sigma_4 \\ \pm\varepsilon_8, & if\ \sigma_4 \leq r_2 < \sigma_5 \\ 0, & if\ r_2 \geq \sigma_5 \end{cases} \quad (3)$$

$$U_{rod-disc}(r_{ij}) = \begin{cases} \infty, & if\ r_2 < \sigma_1 \\ \pm\varepsilon_9, & if\ \sigma_1 \leq r_2 < \sigma_2 \\ \pm\varepsilon_{10}, & if\ \sigma_2 \leq r_2 < \sigma_3 \\ \pm\varepsilon_{11}, & if\ \sigma_3 \leq r_2 < \sigma_4 \\ \pm\varepsilon_{12}, & if\ \sigma_4 \leq r_2 < \sigma_5 \\ 0, & if\ r_2 \geq \sigma_5 \end{cases} \quad (4)$$

where r_{ij} is the distance between two charges and the signs of the potential are negative for unlike charges and positive for like charges. The magnitudes of the energies, $\varepsilon_1 = 2.244$, $\varepsilon_2 = 1.648$, $\varepsilon_3 = 1.088$, $\varepsilon_4 = 0.733$, $\varepsilon_5 = 1.195$, $\varepsilon_6 = 0.785$, $\varepsilon_7 = 0.303$, $\varepsilon_8 = 0.148$, $\varepsilon_9 = 1.556$, $\varepsilon_{10} = 1.063$, $\varepsilon_{11} = 0.633$, $\varepsilon_{12} = 0.192$ as well as the locations for the well boundaries, $\sigma 2 = 0.45\sigma$, $\sigma 3 = 0.595\sigma$, $\sigma 4 = 0.9\sigma$, and $\sigma 5 = 1.10\sigma$ are chosen to approximate the Yukawa potential, which is the screened Coulomb potential. The Yukawa potential, $U(r^*)$, is the potential energy between a pair of charges of opposite signs,[57] and is defined as:

$$U(r^*) = -\varepsilon/r^* \, exp\left(-\kappa^*(r^* - 1)\right) \quad (5)$$

where ε is a constant related to the strength of interaction, κ^* is the reduced inverse Debye length, and r^* is the reduced distance between charges and is defined as $r^* = {}^{r}/_{\sigma}$. We chose parameters for the Yukawa potential based on 20 nm diameter gold nanorods synthesized by Kozek et al.[58] and Maity et al.[36] and suspended in a 10^{-5} M NaCl solution. From these values, we calculate the Debye length, ${}^{1}/_{\kappa}$, to be 96.1 nm using the formula for monovalent electrolytes ${}^{1}/_{\kappa} = 0.304/[NaCl]^{0.5}$, where [NaCl] is the concentration of NaCl. From the Debye length, the reduced Debye length, $\kappa^* = \sigma\kappa$, is 0.208. The reduced temperature for our simulations is $T^* = \alpha k_B T/\varepsilon$, where k_B is the Boltzmann constant, ε is the constant in the Yukawa Potential, and α is 0.864. The value for α is calculated by setting the Yukawa potential in Equation (5) equal to the simplified Coulomb potential, $U_c(r^*) = 1/r^*$, at $r^* = 0.3$ the distance of closest approach for two charged discs in our simulations.

The energy values ε_1 through ε_{12} in Equations (2)-(4) were chosen to fit the continuous Yukawa potential in Equation (5). This was done by calculating the total Yukawa potential between the four charges on two colloids in the configurations shown in Table 1. The energy values of the discontinuous potentials were then selected so that the total discontinuous interaction energy matched as best as possible to the total Yukawa potential. Emphasis was placed on developing a discontinuous potential that would match the interaction energies of the small colloidal aggregates that have been seen in previous experimental and simulation investigations on single-component systems (two colloids in head-to-tail and side-by-side orientations and three discs in a close packed

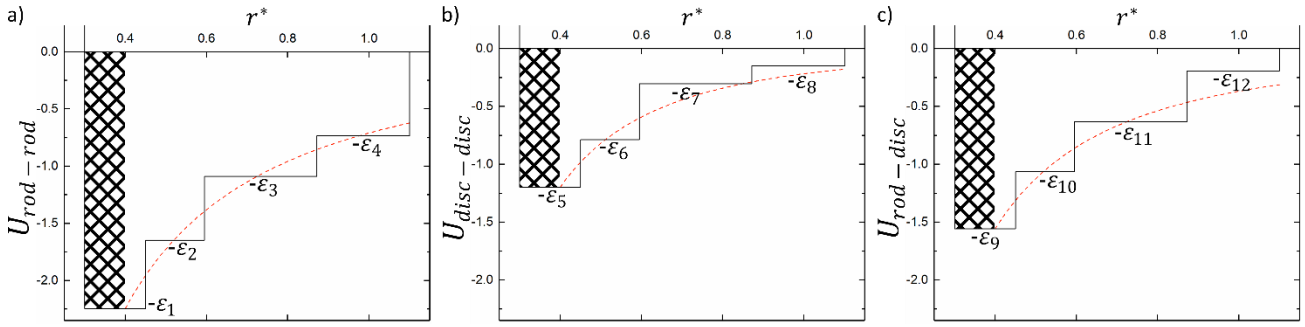

Figure 2: Plot of the discontinuous interaction potential between two charged discs (black) versus the distance between the center of two charges of opposite sign for interactions between charges (a) on two rods, (b) on two discs, or (c) on a rod with a charge on a disc. The total Yukawa potential for the interactions between the four charges on two colloids in a head to tail orientation (red) is shown for comparison.

staggered chain as shown in the first column of Table 1). Figure 2(a)-(c) show the charge-charge discontinuous potentials (black) as a function of the distance between charges (a) on two rods, (b) on two discs, or (c) on one rod and one disc. The total Yukawa potential (red) between the respective colloids aligned head-to-tail as a function of the distance between the closest charges is shown for comparison. The hashed-out regions of the potentials in Figure 2 indicate the areas of the charged discs' energy wells that are inaccessible due to the hard sphere boundary of the hard disc or hard rod on which the charge resides.

The locations of the discontinuities in the potential energy were chosen to highlight structural features commonly seen in dipolar colloids. The first well distance, between σ_1 and σ_2, was chosen to allow the colloids to form head-to-tail chains. The second well distance, between σ_2 and σ_3, gives a region where the colloids can come together at an angle and for the creation of "Y-shaped" junctions. The third well, between and σ_3 and σ_4, describes the interaction between the dipoles in the close packed staggered chain configuration. The fourth well, between and σ_3 and σ_4, describes the region where colloids can come together in a side-by-side orientation.

We chose to compare the charge-charge discontinuous potential to the total Yukawa potential between colloids because, for the majority possible of orientations and configurations between two colloids, the only charges that will "feel" each other in our discontinuous potential are the two charges nearest to each other. Therefore, we designed our discontinuous potential so that two interacting charges would well approximate the total interaction between colloids. However, when two colloids are in a configuration in which a charge on one colloid "feels" both charges on an adjacent colloid, the result is a total discontinuous energy of interaction that is not a monotonic function of the distance between the closest charges. This means that two colloids can become more attractive as they move further apart, falling into local energy minimums. This is particularly true for the dipolar discs because the range of the potential is longer than the diameter of discs. To create a monotonically increasing function of the discontinuous potential energy as a function of the distance between closest charges would have required that the discontinuous potential be cut off at a very short distance to prevent a charge on one colloid from interacting with both charges on an adjacent colloid. The short cutoff would have resulted in a potential that was unable to account for side-by-side and close packed staggered chain interactions. See supplemental information for a detailed discussion of this. To minimize the impact of these local energy minima we ran the simulations for a larger number of collisions to give the colloids time to escape local energy minimums. Additionally, we repeated simulations with a shorter-range potential which minimized occurrence of these local minimums and found substantially the same results as we have presented here.

Table 1: Total interaction energy, Uij, between all pairs of charges for the two- and three- particle configurations shown in the first column. The second column gives the energy of the corresponding configuration based on the Yukawa potential for the four charge-charge interactions between pairs of charges on different colloids. The third column shows the expression for the total discontinuous potential for each configuration based on the energy well cut-offs described by Equations (2)-(4). The fourth column gives the resulting total DMD interaction potential between the four charges based on the expressions in column three.

Configuration	Uij Yukawa Potential	DMD Interactions	Uij DMD Potential
	-2.244	ε_1	-2.244
	-1.120	$\varepsilon_5 - 2\cdot\varepsilon_8$	-0.899
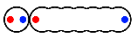	-1.556	$\varepsilon_9 - \varepsilon_{12}$	-1.365
	-1.467	$2\cdot\varepsilon_4$	-1.467
	-0.298	$2\cdot\varepsilon_8$	-0.298
	-0.192	ε_{12}	-0.192
	-0.911	$\varepsilon_5 + 2\cdot\varepsilon_7 - 6\cdot\varepsilon_8$	-0.911

Methods

We performed simulations on two mixtures of dipolar rods and discs: one in which the numbers of rods and discs are equal ("equal number mixture"), and the other in which the areas of the rods (ϕ_R) and discs (ϕ_D) are equal ("equal area mixture"). In the equal number mixture, there were $N_R = 500$ dipolar rods and $N_D = 500$ dipolar discs. In the equal area mixture, there were $N_R = 500$ rods and $N_D = 2328$ discs. Detailed discussion of the results for single component dipolar discs and dipolar rods can be found in the work by Schmidle et al.[31] and by Rutkowski et al.[40] respectively. Because the discontinuous potentials used in those two papers were slightly different than is used in the current investigation, we have performed single-component

simulations containing either 500 dipolar rods or 500 dipolar discs to allow for direct comparison of phase boundaries and structures formed by mixtures to those found in the single-component systems.

Discontinuous molecular dynamics (DMD) simulations are carried out in a square 2-d simulation box with periodic boundary conditions in the NVT ensemble. DMD simulations proceed by calculating the forces acting on particles only when particles are separated by a distance that corresponds to a discontinuity in the potential, making DMD a fast alternative to traditional molecular dynamics. Constant temperature is achieved using the Andersen thermostat, which is implemented by periodically selecting a random particle to undergo a collision with a "ghost" particle.[59] The collisions with the "ghost" particle creates a system whose temperature has a Boltzmann distribution around the set temperature. The simulations are carried out by using a simulated annealing process. The simulated annealing process proceeds by heating colloids at a fixed area fraction ($\phi \equiv \phi_R + \phi_D$) at a high temperature, $T^* = 0.6$, for approximately four billion collisions to obtain a random configuration. After this, the random configuration is cooled in discrete temperature steps, each lasting for one billion collisions with data collected every five million collisions over the final seven hundred million steps before moving on to the next step. This sampling rate results in 140 configurations at each temperature, which are used in determining phase transitions. Large temperature steps are used at high temperature since the colloids readily reach equilibrium when little or no aggregation is occurring. We use smaller temperature steps at lower reduced temperatures to allow the colloids to reach equilibrium. These small steps allow us to accurately capture the aggregation behavior. Three simulated annealing simulations were performed for each system, and data is averaged over these three runs.

To quantify the extent of aggregation of the dipolar colloids in our simulations, we define polymerization and clustering criteria. A pair of colloids is considered to be polymerized if a charge on one colloid lies within 1.1σ of an opposite charge on the other. This distance corresponds to the outermost energy well of our discontinuous potential. Two colloids polymerized in this manner would be considered a cluster of two particles. If a charge on a third colloid is also within 1.1σ of an opposite charge on a colloid in a polymerized pair, then all three colloids will be in the same cluster. If the charges have the same sign they are not considered to be in a cluster since this would be a repulsive interaction.

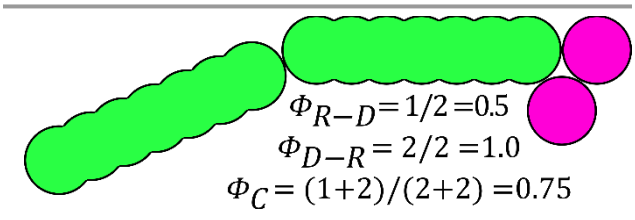

Figure 3: Examples of Φ_{R-D}, Φ_{D-R}, and Φ_C calculations for a simple four particle system.

The extent of polymerization, $\Phi(T^*)$, is a measure of how many colloids have polymerized with at least one other colloid. It is defined as the ensemble average of the number of colloids that have polymerized, N_a, divided by the total number of colloids in the simulation box, N.

$$\Phi(T^*) = \langle N_a/N \rangle \quad (6)$$

We define four parameters: $\Phi_{R-R}(T^*)$, $\Phi_{D-D}(T^*)$, $\Phi_{R-D}(T^*)$, and $\Phi_{D-R}(T^*)$ to calculate the extent that rods have polymerized with other rods, discs have polymerized with other discs, rods have polymerized with discs, respectively.

$$\Phi_{R-R}(T^*) = \langle N_{R-R}/N_R \rangle \quad (7)$$

$$\Phi_{D-D}(T^*) = \langle N_{D-D}/N_D \rangle \quad (8)$$

$$\Phi_{R-D}(T^*) = \langle N_{R-D}/N_R \rangle \quad (9)$$

$$\Phi_{D-R}(T^*) = \langle N_{D-R}/N_D \rangle \quad (10)$$

where $N_{R\text{-}R}$ is the number of rods that polymerize with at least one other rod, $N_{D\text{-}D}$ is the number of discs that polymerize with at least one other disc, $N_{R\text{-}D}$ is the number of rods that polymerize with at least one disc and $N_{D\text{-}R}$ is the number of discs that polymerize with at least one rod. Note that $N_{R\text{-}D}$ is not the same as $N_{D\text{-}R}$ as seen in Figure 3.

We also define a fifth parameter: $\Phi_C(T^*)$ is the sum of the number of rods that have polymerized with discs and the number of discs that have polymerized with rods divided by the total number of particles.

$$\Phi_C(T^*) = \langle (N_{R-D} + N_{D-R})/N \rangle \quad (11)$$

When the extent of polymerization in Equations (7)-(11) is close to zero it means that the colloids are in the fluid phase. When $\Phi(T^*)$ is close to 1 it means the colloids have polymerized and have formed a string fluid.

We plot the extents of polymerization given in Equations (7) and (8) versus temperature at each area fraction to find the transition temperature between a fluid and string fluid as shown for example in the inset of Figure 4. The general trend for $\Phi_{R-R}(T^*)$ and $\Phi_{D-D}(T^*)$ at low ϕ is that at high temperatures the extent of polymerization is low, and as the temperature is lowered the extent of polymerization rises rapidly, plateauing near 1. The rod fluid to rod string-fluid transition temperature is defined to be the T^* value at the inflection point in the curve fitted to the $\Phi_{R-R}(T^*)$ versus T^* data. The disc fluid to disc string-fluid transition temperature is defined to be the T^* value at the inflection point in the curve fitted to the $\Phi_{D-D}(T^*)$ versus T^* data. At these temperatures the colloids go from a disordered fluid to a string-fluid consisting of small clusters of rods (Equation (7)) or discs (Equation (8)). This definition for the fluid to string-fluid transition temperature works well at low area fractions where the fluid phase (low extent of polymerization) is evident. At higher area fractions, however, the values of $\Phi_{R-R}(T^*)$ and $\Phi_{D-D}(T^*)$ are large (> 0.8) even at high temperature, which indicates that most of the colloids are already clustered and no clear fluid

phase can be discerned by examining the extent of polymerization. Therefore, instead of transitioning from a fluid to a string-fluid, the colloids undergo a transition from a state where most are clustered to a state where all are clustered at high area fractions.

To determine when the colloids undergo a transition from a string-fluid phase to a "gel" phase, we measure the percolation probability, $\Pi(T^*)$. The percolation probability gives the probability of finding a network that is percolated, where percolation is defined as a cluster that spans the simulation box and connects back to itself through the periodic boundaries. We note that percolation is a prerequisite for gelation, but it is not sufficient by itself to declare a system a gel (which also has specific dynamic properties).[40] The percolation probability is defined as:

$$\Pi(T^*) = \langle C_{per}/C \rangle \quad (12)$$

where C_{per} is the number of percolated particle configurations at a temperature T^* and C is the total number of configurations measured at that temperature. The percolation temperature (the temperature at which a system undergoes a transition between a system that is not percolated and one that is percolated) is defined to be the T^* value at the inflection point of a curve fitted to a plot of percolation probability versus reduced temperature.[60]

Results

Fluid phases

At high T^* the dipolar colloids form a disordered fluid phase as seen in simulations of hard sphere and hard rod models. We do not see any entropically driven phase separation into rod-rich and disc-rich phases at the area fractions investigated. Additionally, the aspect ratio of the rods in our model are below the aspect ratio at which we would expect to see the liquid crystal nematic or smectic phases. As we will see below, the colloids begin to cluster as the temperature is lowered and the shape anisotropy and dipolar anisotropic interactions both become important.

Disc-Disc and Rod-Rod Polymerization

The first transition that the mixtures undergo as the temperature is lowered at fixed area fraction is from a disordered fluid to a string-fluid. The string-fluid phase consists of short chains of clustered colloids. We compare the mixtures' fluid to string-fluid transition temperatures for each area fraction simulated to that of the single component reference systems in Figure 4. Looking first at the behavior of the dipolar discs (blue curves), we see that the transition from a fluid to a disc string-fluid occurs at an approximately constant T^* as area fraction is increased for both mixtures considered in this paper. Additionally, the fluid to disc string-fluid transition occurs at lower reduced temperature in the mixtures than for single-component dipolar discs, particularly at high area fractions. From this we conclude that the addition of dipolar rods to a system of dipolar discs greatly suppresses the formation of the disc string-fluid. Next, we consider the behavior of the dipolar

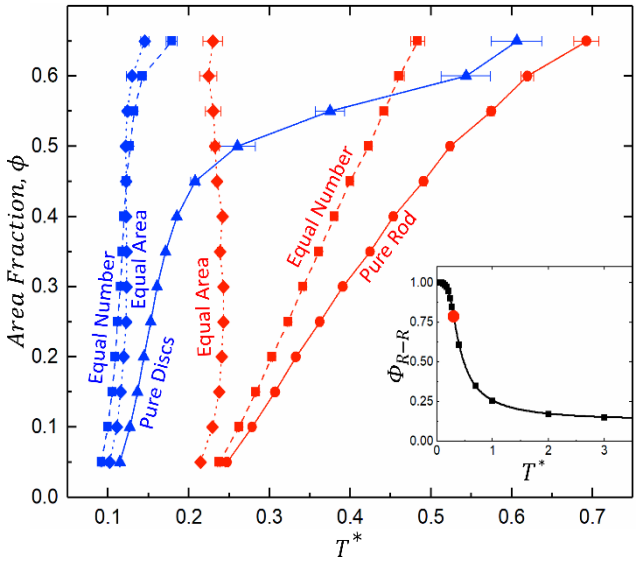

Figure 4: Transition from fluid to string-fluid as T^* decreases for dipolar rods (red) and dipolar discs (blue) for simulations of an equal number of rods and discs (squares), an equal area of rods and discs (diamonds), only discs (triangles) or only rods (circles). The inset shows the curve fitted to extent of rod-rod polymerization versus temperature data (black squares) for an equal number mixture at $\phi = 0.20$; this curve is characteristic of all the rod-rod and disc-disc extents of polymerization seen in the mixtures. The inflection point of the fitted curve is marked (red circle).

rods (red). For the equal area mixture, the fluid to rod string-fluid transition occurs at an approximately constant T^* as area fraction is increased, and this T^* is significantly lower than the transition temperature for pure rods. The equal number mixture exhibits a fluid to rod string-fluid transition at lower T^* than pure rods, but not as low as for the equal area mixture. The equal number fluid to rod string-fluid transition occurs at higher T^* as area fraction increases, following a linear trend like that seen for dipolar rods. From this we conclude that a significant number of discs need to be added to dipolar rods to have a marked impact on rod polymerization.

Rod-Disc Polymerization

The rod-disc extent of polymerization for both mixtures displays much more complex behavior than seen in either the rod-rod or disc-disc extents of polymerization. See for example the comparison of the $\Phi_{R-D}(T^*)$, $\Phi_{D-R}(T^*)$, $\Phi_C(T^*)$ and $\Phi_{D-D}(T^*)$ versus T^* curves in Figure (a) for the equal number mixture. At high T^* the rod-disc extent of polymerization is greater than the disc-disc extent of polymerization. The rod-disc extent of polymerization increases at T^* decreases until it reaches a local maximum value, which occurs when $\Phi_{R-D}(T^*) \cong \Phi_{D-D}(T^*)$. Thereafter, $\Phi_{D-D}(T^*)$ rises rapidly as T^* decreases, while $\Phi_{R-D}(T^*)$ decreases until it reaches a local minimum which occurs at approximately the same temperature as the inflection point in the disc-disc extent of polymerization. After this, $\Phi_{R-D}(T^*)$ again grows as T^* is lowered until the end of the simulated annealing procedure. In the equal number mixture, the values of $\Phi_{D-R}(T^*)$ and $\Phi_C(T^*)$ closely match those of $\Phi_{R-D}(T^*)$.

The behavior of the rod-disc extent of polymerization in the equal number mixture can be explained by examining snapshots of simulations as temperature is reduced. The snapshot in Figure (b) depicts an equal number mixture at the temperature

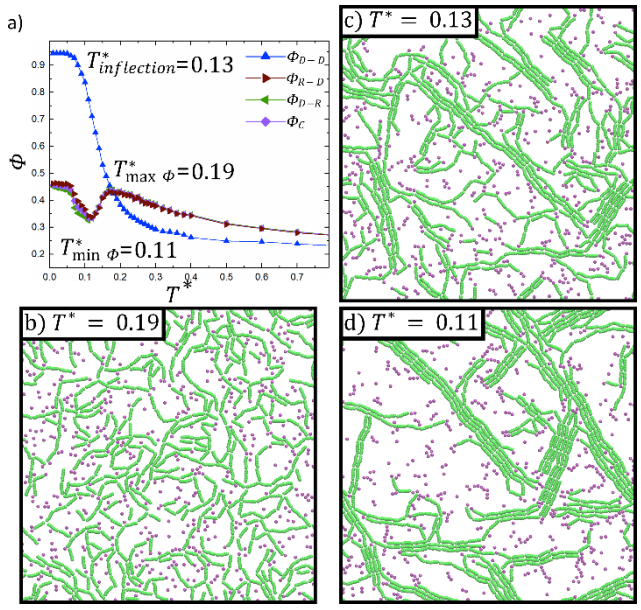

Figure 5: (a) Comparison between disc-disc (blue), rod-disc (brown), disc-rod (green), and combined (purple) extent of polymerization for an equal number mixture at ϕ = 0.30. DMD simulation snapshots at (b) $T^* = 0.19$, the maximum in Φ_{R-D}, (c) $T^* = 0.13$, the inflection point in Φ_{D-D}, and (d) $T^* = 0.11$, thin minimum in Φ_{R-D}. Dipolar rods are shown in green and dipolar discs are shown in purple.

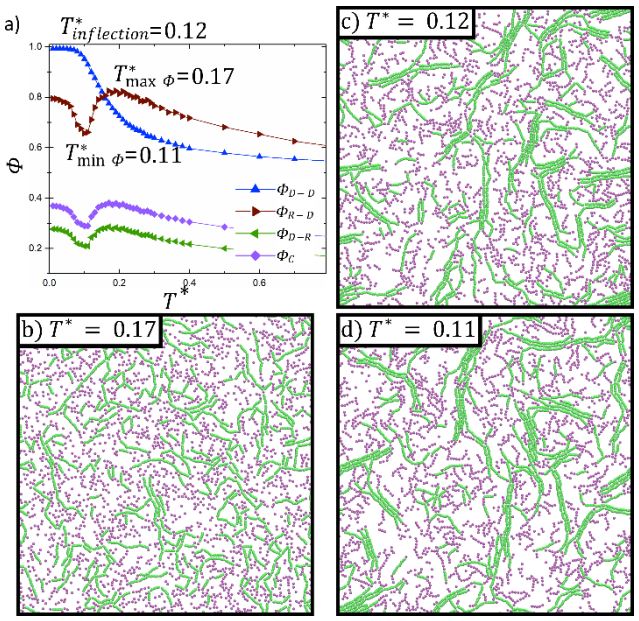

Figure 6: (a) Comparison between disc-disc (blue), rod-disc (brown), disc-rod (green), and combined (purple) extent of polymerization for an equal area mixture at ϕ = 0.30. DMD simulation snapshots at (b) $T^* = 0.17$, the maximum in Φ_{R-D}, (c) $T^* = 0.12$, the inflection point in Φ_{D-D}, and (d) $T^* = 0.11$, thin minimum in Φ_{R-D}. Dipolar rods are shown in green and dipolar discs are shown in purple.

at which $\Phi_{R-D}(T^*)$ is a maximum. In this figure, we see a loose network of chains of dipolar rods that are aligned head-to-tail. Most rod-disc polymerized pairs observed at this temperature have the rods and discs at a distance that corresponds to the third energy well, indicating that the discs have polymerized at the junctions between two head-to-tail aligned rods. Below this temperature, as shown in Figure (c), the clustering between rod and discs is reduced in favor of coarse strands of rods that come together through side-by-side interactions. The formation of coarse chains of head-to-tail aligned rods limits the number of sites available for forming head-to-tail aligned rod-disc pairs, even though this interaction is stronger than head-to-tail aligned discs. At this temperature, the beginning of the formation of a disc-disc string-fluid phase in the voids between the chains of rods is also apparent. As the temperature is reduced to that at which $\Phi_{R-D}(T^*)$ is a minimum, Figure (d), just below the formation of the disc-string-fluid, we can see a large number of short disc-disc chains with a few of these disc strings tethered to a network primarily formed by rods.

The behavior of the rod-disc polymerization in the equal area mixture, shown in Figure (a), mirrors that of the rod-disc polymerization in the equal number mixture with the notable exception that significantly more of the rods are polymerized with at least one disc. The snapshots in Figure 6: (a) Comparison between disc-disc (blue), rod-disc (brown), disc-rod (green), and combined (purple) extent of polymerization for an equal area mixture at ϕ = 0.30. DMD simulation snapshots at (b) $T^* = 0.17$, the maximum in Φ_{R-D}, (c) $T^* = 0.12$, the inflection point in Φ_{D-D}, and (d) $T^* = 0.11$, thin minimum in Φ_{R-D}. Dipolar rods are shown in green and dipolar discs are shown in purple. show that as the equal area system cools, the dipolar rods exhibit chain formation and coarsening behavior that is similar to that seen in the equal number system, but to a lesser extent. This leaves many sites available for the formation of head-to-tail aligned rod-disc pairs. The sum of the number of rod-to-disc and disc-to-rod polymerizations, $\Phi_C(T^*)$, remains low due to the large number of discs in the system.

The complex behavior exhibited by $\Phi_{R-D}(T^*)$ makes it difficult to define when the mixtures exhibit rod-disc polymerization as we did for rod-rod and disc-disc polymerization where we looked for inflections points in $\Phi_{R-R}(T^*)$ and $\Phi_{D-D}(T^*)$. There is no clear string-fluid phase where the strings are composed of small chains of rods and discs bonded to each other. Instead we use $\Phi_C(T^*)$ to gain information about the structure of the percolated networks. We define the transition from a percolated network made primarily of rods to a percolated network that consists of large numbers of rods and discs. The temperature at which this transition occurs is found by finding the inflection point in a curve fit to $\Phi_C(T^*)$ in the region between $T^* = 0.1$ and the local minimum.

"Gel" Phases and Percolation

We compare area fraction vs. percolation temperature curves of the two mixtures to those of the two single-component references in Figure (a). All four systems follow the general trend that at low area fraction the systems percolate at low T^*, and as area fraction increases, the percolation temperature also increases. For low area fractions, $\phi < 0.4$, $T_{perc}(\text{pure rods}) > T_{perc}(\text{EN}) > T_{perc}(\text{EA}) > T_{perc}(\text{pure discs})$. Additionally, each system has a characteristic area fraction above which it is not possible to calculate a percolation phase transition (ϕ_{max}) because the system percolates even at high temperatures. This point occurs at $\phi_{max} = 0.45$ for the pure dipolar discs, $\phi_{max} = 0.50$ for the

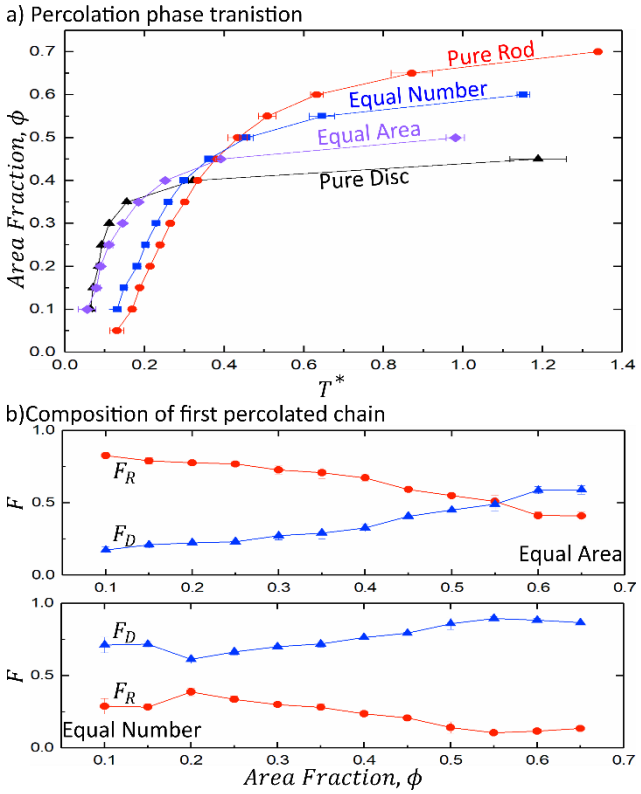

Figure 7: (a) Transition from non-percolated network to percolated network as temperature is reduced for dipolar rods (red), equal number rods and discs (blue), equal area rods and discs (purple) and dipolar discs (black). (b) The fraction of rods (red), and the fraction of discs (blue) in the first percolated chain at each area fraction for the equal number mixture (top) and the equal area mixture (bottom).

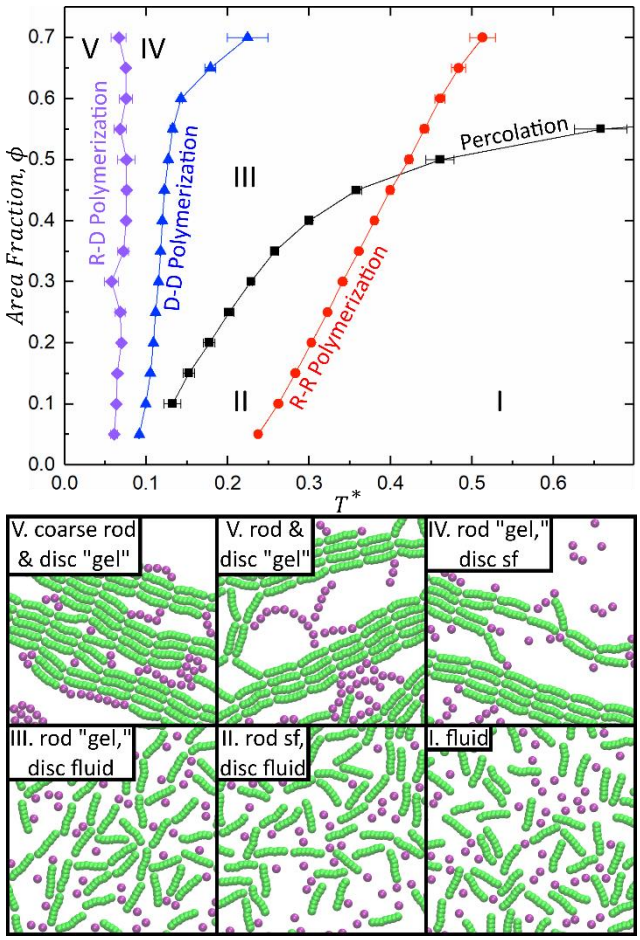

Figure 8: Phase diagram for a mixture of equal number of dipolar rods and discs plotted in the area fraction vs. temperature plane. Fluid (I), rod string-fluid with disc fluid (II), rod "gel" with disc fluid (III), rod "gel" with disc string-fluid (IV), and rod and disc "gel" (V) phases are present. Zoomed-in sections of the full simulation cell are shown to highlight the structural differences between the phases. See supplemental information for images of the full simulation cell.

equal area mixture, $\phi_{max} = 0.60$ for the equal number mixture, and $\phi_{max} = 0.70$ for the pure dipolar rods. These values suggest that a mixture will have a lower value of ϕ_{max} as the area occupied by discs increases relative to the area occupied by rods, or, to put it conversely, ϕ_{max} increases as rods are added to a system.

We gain more insight into the structure of the percolated networks formed by the mixtures when we analyze the composition of the first percolated chain at each area fraction (in each run). We define F_R (F_D) as the number of rods (number of discs) in the first percolated chain divided by the total number of colloids in the first percolated chain. We compare the percolation temperatures of the pure rod reference to the equal number mixture. We see that for $\phi < 0.55$ the systems percolate at similar T^*, but above $\phi = 0.55$ the percolation temperatures diverge with the mixture percolating at a higher T^* Figure (a). The plot of FR and FD versus area fraction for the equal number mixture, Figure (b, top), shows that for $\phi \leq 0.50$, the first percolated network is primarily composed of rods, but above $\phi = 0.55$, FD > FR. Next, we compare the percolation temperatures of the pure disc reference to the equal area mixture. We see that for $\phi < 0.35$ the systems percolate at similar T^*, but above $\phi = 0.45$ the percolation temperatures diverge with the pure discs percolating at a higher T^*. The plot of FR and FD versus area fraction for the equal number mixture, Figure (b, bottom), shows that FD > FR for all area fractions.

From the above observations, we draw two conclusions about the percolation behavior of mixtures. The first conclusion that we make is that rods play a key role in percolation at low area fraction. A mixture in which rods are present in abundance ($\phi_R \gg \phi_D$) will percolate at higher T^* then a mixture where $\phi_R = \phi_D$. When rods make up the bulk of the occupied area, there is a greater chance for pairs of rods to interact, and these interactions are more likely to form clusters because of the stronger energy of interaction between pairs of rods then between rods and discs or pairs of discs. This results in system-spanning clusters that contain many rods and few discs as seen in the equal number mixture. The second conclusion we make is that discs play a key role in percolation at high area fractions. At high ϕ in both mixtures, the first percolated network was primary composed of discs. This could be due to the dipolar discs having a smaller excluded area than the dipolar rods, which makes it easier for the discs to arrange in attractive configurations at high area fraction where jamming could occur. An analysis of the pore size distribution in the "gel" phases below percolation shows that at constant area fraction, the probability of finding a given pore size decreases monotonically with pore size, with no characteristic pore size. Additionally, as ϕ increases, there is a decreased probability of finding large pores.

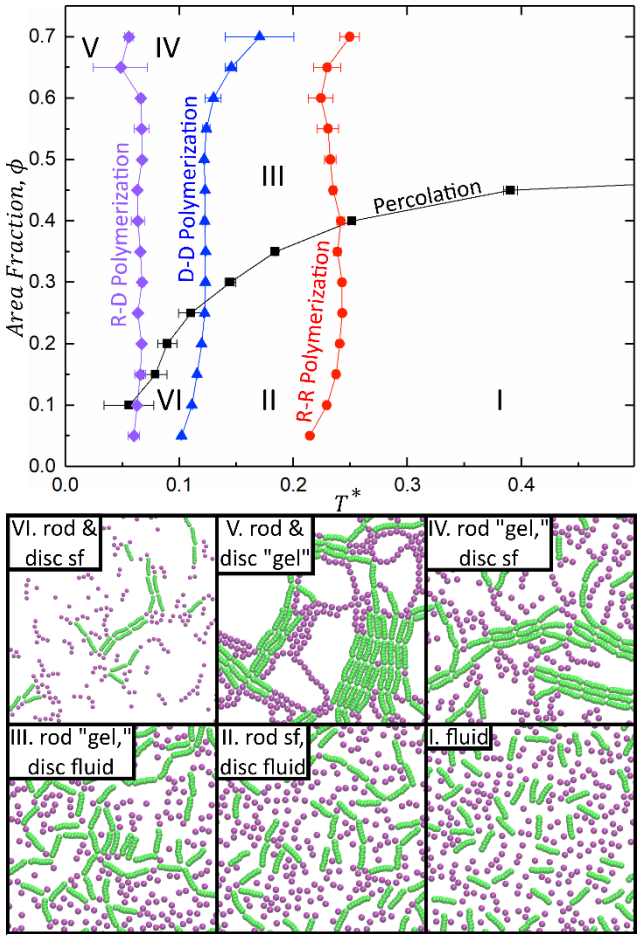

Figure 9: Phase diagram for a mixture of equal area of dipolar rods and discs plotted in the area fraction vs. temperature plane. Fluid (I), rod string-fluid with disc fluid (II), rod "gel" with disc fluid (III), rod "gel" with disc string-fluid (IV), rod and disc "gel," (V) and rod and disc string-fluid (IV) phases are present.

Phase Diagram: Equal Number Case

The phase transitions for the equal number mixture are summarized in a phase diagram in the area fraction versus temperature plane, Figure . As the system is slowly cooled starting from a reduced temperature of 6.0, the first transition that occurs is from a fluid (labeled "I" in Figure) to a rod string-fluid (II) which is characterized by small clusters of dipolar rods, arranged primarily in head-to-tail orientations. There are very few clusters of discs with other discs, or of rods and discs. Next the rod-string fluid transitions to a rod "gel," (III) a percolated network that is primarily composed of dipolar rods clustered to each other in a head-to-tail orientation. As discussed in the section on rod-disc polymerization there are some discs incorporated into the percolated network, primarily serving as junctions between clusters of rods or as the terminating colloid in a chain of rods. As the system is further cooled, the rod "gel" begins to coarsen through side-by-side chain interactions, and the discs that were clustered with rods begin to break away from the rod "gel" and form their own clusters; a disc string-fluid (IV). The final transition occurs when the disc string-fluid gets incorporated into the rod "gel" to form a rod and disc "gel" (V). When this rod and disc "gel" initially forms it is characterized by short chains of dipolar discs attached to a large, coarse network of dipolar rods. Upon further cooling the dipolar short chains of dipolar discs condense into clusters of discs with hexagonal order.

Phase Diagram: Equal Area Case

The phase transitions for the equal area mixture are summarized in a phase diagram in the area fraction versus temperature plane, Figure 9. Note that there are ~4.5 times as many discs as rods in this system. Most of the phases seen in this mixture are similar to those in the equal number mixture, although there are noticeable differences. The rod "gel" that forms in regions III and IV of the equal area phase diagram contains a significantly greater number of dipolar discs than in the corresponding regions for the equal number mixture. The rod and disc "gel" (V) that forms at very low temperature consists of discrete clusters of rods connected to each other through clusters of discs instead of the large, system-spanning rod cluster in the equal number mixture. Finally, the equal area mixture has an additional phase (VI) that occurs at low area fractions and consists of both a rod string-fluid and a disc string-fluid, with few of the strings containing both rods and discs.

Discussion and conclusions

We have calculated phase diagrams for equal-area and equal-number mixtures of dipolar colloidal rods and dipolar colloidal discs using discontinuous molecular dynamics simulations where the charge-charge discontinuous potential approximates the Yukawa potential. The structures displayed by these mixtures included fluid, string-fluid, and "gel" phases. Additionally, we see separation between the two species: rods preferring to polymerize with other rods, discs polymerizing with other discs, but significantly fewer instances of rods polymerizing with discs. This gives rise to states where dipolar rods exist primarily in one structure and dipolar discs in a second structure, for instance state III in Figure and Figure 9 where the rods form a "gel" while the discs remain interspersed as a fluid. We compare the transitions of the two mixtures to those found for pure dipolar rods and pure dipolar discs. Through this comparison we see that the addition of a small number of dipolar rods to pure dipolar discs suppresses dipolar disc polymerization, however the addition of a small number of dipolar discs to pure dipolar rods does not significantly impact dipolar rod polymerization. Dipolar rod polymerization is suppressed only when a large number of dipolar discs are added to the pure rod system.

Our results reveal complex phase behavior that arises in mixtures of mutually attractive colloidal particles. We have focused on the case where the rods and discs are of similar size so that structure formation is driven by dipolar interactions and not entropic effects. We find that mixtures of dipolar rods and discs follow a general assembly pathway that begins with the formation of energetically favorable head-to-tail chains of rods. Once the rods form long chains with each other, there are a limited number of sites available to form chains of mixed rods and discs aligned head-to-tail. Because of this, the next step in the assembly pathway is that discs begin to form head-to-tail

aligned chains with other discs. The final step in the general assembly pathway is that chains of rods and discs interact through side-by-side and close packed staggered chain interactions, which causes branching and coarsening of chains. Knowledge of this general pathway helps us to understand how the assembly of mixtures is impacted by the mixture composition, strength of interaction between species, and the temperature. Mixtures that have a large area fraction of rods relative to the area fraction of discs could be used to form gels that encapsulate the discs, and this could have useful for drug delivery applications. Mixtures with an equal area fraction of rods and discs could have interesting rheological properties as they could contain gels that have separate domains for rod rich and disc rich clusters.

The phase diagrams calculated in this work can aid experimentalists in understanding the complex aggregation behavior seen in colloidal mixtures. The phase separation induced through different strengths of attractive and repulsive interactions exhibited between colloids of different shapes in our model could offer a new avenue to control colloidal aggregation. Dipolar particles can be created from different shapes and materials that, when mixed together, could create novel temperature-sensitive surface coatings that take advantage of the fact that different particle types form clusters at different temperature. In three dimensions these mixtures could form networks similar to the bicontinuous gels seen in mixtures of dipolar spheres of different sizes,[45] however it is difficult to predict how head-to-tail aligned chains of dipolar rods would form side-by-side interactions with each other. Further study in this area would be of interest.

Our use of DMD was driven by our desire to quickly explore the phase space for these mixtures so as to provide insight to experimentalists about the conditions necessary to form phases that may be of interest. The advantage of DMD is that we can simulate many systems with modest computational resources compared to the traditional techniques such as molecular dynamics used with a continuous potential. Our choice of a short-range potential was driven by our focus on replicating the environment found in high salt concentrations where charge-charge interactions are screened by electrolytes. Simulation results using similar short-range discontinuous potentials have shown good qualitative agreement with both experimental results for dipolar spheres and results from simulations on dipolar spheres that account for true dipolar interactions more rigorously. An additional benefit of the short-range discontinuous potential is that accounting for long-range interactions is often the most time-consuming part of a simulation involving a continuous potential. Several other sets of discontinuous potentials designed and used in simulations to verify the results obtained using the potentials summarized by Equations (2)-(4). These potentials varied from the one reported in this paper by changing the number of steps in the potential, the location of boundaries between steps, and the energy values of each step. The phase diagrams calculated based on these other potentials largely agree with the above results. There were, however, some differences in the local structures formed by these other potentials. If the first well (representing the strongest interaction energy) was broad, the colloids would form more "Y-shaped" junctions and fewer head-to-tail chains, resulting in the dipolar rods forming a structure similar to that of a triangular truss instead of the structures depicted in Figure Figure 9. If additional steps were included beyond 1.1σ, the colloids formed "staggered chains," such as those found in magnetic Janus particles, where adjacent beads on the same side of the chain do not touch.[61]

Conflicts of interest

There are no conflicts to declare.

Acknowledgements

This work was supported by NSF's Research Triangle MRSEC under grant number DMR-1121107, CBET-1512059, and OISE-1065466. It was also supported by the German Research Foundation (DFG) through grant IRTG 1524. We would also like to thank Drs. David Rutkowski and Orlin Velev for helpful discussions.

Notes and references

1 F. Caruso, R. Caruso and H. Mohwald, *Science,* 1998, **282**, 1111-1114 (DOI:10.1126/science.282.5391.1111).
2 S. Mitragotri and J. Lahann, *Nat. Mater.,* 2009, **8**, 15-23 (DOI:10.1038/NMAT2344).
3 D. A. Giljohann, D. S. Seferos, W. L. Daniel, M. D. Massich, P. C. Patel and C. A. Mirkin, *Angew. Chem. -Int. Edit.,* 2010, **49**, 3280-3294 (DOI:10.1002/anie.200904359).
4 A. Hynninen, J. H. J. Thijssen, E. C. M. Vermolen, M. Dijkstra and A. Van Blaaderen, *Nature Materials,* 2007, **6**, 202-205 (DOI:10.1038/nmat1841).
5 J. Baumgartl, M. Zvyagolskaya and C. Bechinger, *Phys. Rev. Lett.,* 2007, **99**, 205503 (DOI:10.1103/PhysRevLett.99.205503).
6 Y. Li, W. Cai and G. Duan, *Chemistry of Materials,* 2008, **20**, 615-624 (DOI:10.1021/cm701977g).
7 S. Kredentser, O. Buluy, P. Davidson, I. Dozov, S. Malynych, V. Reshetnyak, K. Slyusarenko and Y. Reznikov, *Soft Matter,* 2013, **9**, 5061-5066 (DOI:10.1039/c3sm27881f).
8 D. J. Milliron, S. M. Hughes, Y. Cui, L. Manna, J. B. Li, L. W. Wang and A. P. Alivisatos, *Nature,* 2004, **430**, 190-195 (DOI:10.1038/nature02695).
9 Y. Chen, X. Ding, S. S. Lin, S. Yang, P. Huang, N. Nama, Y. Zhao, A. A. Nawaz, F. Guo, W. Wang, Y. Gu, T. E. Mallouk and T. J. Huang, *Acs Nano,* 2013, **7**, 3306-3314 (DOI:10.1021/nn4000034).
10 C. L. Phillips, E. Jankowski, B. J. Krishnatreya, K. V. Edmond, S. Sacanna, D. G. Grier, D. J. Pine and S. C. Glotzer, *Soft Matter,* 2014, **10**, 7468-7479 (DOI:10.1039/c4sm00796d [doi]).
11 J. Smay, J. Cesarano and J. Lewis, *Langmuir,* 2002, **18**, 5429-5437 (DOI:10.1021/la0257135).
12 Y. Huang, X. Duan, Y. Cui, L. Lauhon, K. Kim and C. Lieber, *Science,* 2001, **294**, 1313-1317 (DOI:10.1126/science.1066192).
13 Y. Cui, Q. Wei, H. Park and C. Lieber, *Science,* 2001, **293**, 1289-1292 (DOI:10.1126/science.1062711).
14 J. J. Benkoski, R. M. Deacon, H. B. Land, L. M. Baird, J. L. Breidenich, R. Srinivasan, G. V. Clatterbaugh, P. Y. Keng and J. Pyun, *Soft Matter,* 2010, **6**, 602-609 (DOI:10.1039/b918215b).

15 A. Dinsmore, M. Hsu, M. Nikolaides, M. Marquez, A. Bausch and D. Weitz, *Science,* 2002, **298**, 1006-1009 (DOI:10.1126/science.1074868).
16 S. Tripp, S. Pusztay, A. Ribbe and A. Wei, *J. Am. Chem. Soc.,* 2002, **124**, 7914-7915 (DOI:10.1021/ja0263285).
17 S. Tripp, R. Dunin-Borkowski and A. Wei, *Angewandte Chemie-International Edition,* 2003, **42**, 5591-5593 (DOI:10.1002/anie.200352825).
18 O. Cayre, V. Paunov and O. Velev, *Journal of Materials Chemistry,* 2003, **13**, 2445-2450 (DOI:10.1039/b308817k).
19 G. N. Patey, D. Levesque and J. J. Weis, *Mol. Phys.,* 1979, **38**, 219-239 (DOI:10.1080/00268977900101621).
20 M. Osipov, P. Teixeira and M. daGama, *Physical Review E,* 1996, **54**, 2597-2609 (DOI:10.1103/PhysRevE.54.2597).
21 T. Tlusty and S. Safran, *Science,* 2000, **290**, 1328-1331 (DOI:10.1126/science.290.5495.1328).
22 S. Kantorovich and A. Ivanov, *J Magn Magn Mater,* 2002, **252**, 244-246 (DOI:10.1016/S0304-8853(02)00651-0).
23 S. Kantorovich, A. O. Ivanov, L. Rovigatti, J. M. Tavares and F. Sciortino, *Phys. Rev. Lett.,* 2013, **110**, 148306 (DOI:10.1103/PhysRevLett.110.148306).
24 J. J. Weis and D. Levesque, *Phys. Rev. Lett.,* 1993, **71**, 2729-2732 (DOI:10.1103/PhysRevLett.71.2729).
25 P. Camp, J. Shelley and G. Patey, *Phys. Rev. Lett.,* 2000, **84**, 115-118 (DOI:10.1103/PhysRevLett.84.115).
26 A. Yethiraj and A. van Blaaderen, *Nature,* 2003, **421**, 513-517 (DOI:10.1038/nature01328).
27 S. Klapp, *Journal of Physics-Condensed Matter,* 2005, **17**, R525-R550 (DOI:10.1088/0953-8984/17/15/R02).
28 P. D. Duncan and P. J. Camp, *Phys. Rev. Lett.,* 2006, **97**, 107202 (DOI:10.1103/PhysRevLett.97.107202).
29 L. Rovigatti, J. Russo and F. Sciortino, *Phys. Rev. Lett.,* 2011, **107**, 237801 (DOI:10.1103/PhysRevLett.107.237801).
30 A. Sreekumari and P. Ilg, *Physical Review E,* 2013, **88**, UNSP 042315 (DOI:10.1103/PhysRevE.88.042315).
31 H. Schmidle, C. K. Hall, O. D. Velev and S. H. L. Klapp, *Soft Matter,* 2012, **8**, 1521-1531 (DOI:10.1039/c1sm06576a).
32 J. Jordanovic, S. Jäger and S. H. L. Klapp, *Phys. Rev. Lett.,* 2011, **106**, 038301 (DOI:10.1103/PhysRevLett.106.038301).
33 S. Jäger and S. H. L. Klapp, *Soft Matter,* 2011, **7**, 6606-6616 (DOI:10.1039/c1sm05343d).
34 P. G. Bolhuis, A. Stroobants, D. Frenkel and H. N. W. Lekkerkerker, *J. Chem. Phys.,* 1997, **107**, 1551-1564 (DOI:10.1063/1.474508).
35 H. Zhang, J. K. Nunes, S. E. A. Gratton, K. P. Herlihy, P. D. Pohlhaus and J. M. DeSimone, *New Journal of Physics,* 2009, **11**, 075018 (DOI:10.1088/1367-2630/11/7/075018).
36 S. Maity, W. Wu, C. Xu, J. B. Tracy, K. Gundogdu, J. R. Bochinski and L. I. Clarke, *Nanoscale,* 2014, **6**, 15236-15247 (DOI:10.1039/c4nr05179c).
37 C. W. Shields, S. Zhu, Y. Yang, B. Bharti, J. Liu, B. B. Yellen, O. D. Velev and G. P. Lopez, *Soft Matter,* 2013, **9**, 9219-9229 (DOI:10.1039/c3sm51119g).
38 D. Fava, Z. Nie, M. A. Winnik and E. Kumacheva, *Adv Mater,* 2008, **20**, 4318-4322 (DOI:10.1002/adma.200702786).
39 J. Yan, K. Chaudhary, S. C. Bae, J. A. Lewis and S. Granick, *Nature Communications,* 2013, **4**, 1516-1516 (DOI:10.1038/ncomms2520).
40 D. M. Rutkowski, O. D. Velev, S. H. L. Klapp and C. K. Hall, *Soft Matter,* 2016, **12**, 4932-4943 (DOI:10.1039/c6sm00317f).
41 D. M. Heyes, *Mol. Phys.,* 1992, **77**, 29-44 (DOI:10.1080/00268979200102291).
42 W. Lin, M. Kobayashi, M. Skarba, C. Nu, P. Galletto and M. Borkovec, *Langmuir,* 2006, **22**, 1038-1047 (DOI:10.1021/la0522808).
43 B. Bharti, J. Meissner and G. H. Findenegg, *Langmuir,* 2011, **27**, 9823-9833 (DOI:10.1021/la201898v).
44 B. Bharti, G. H. Findenegg and O. D. Velev, *Langmuir,* 2014, **30**, 6577-6587 (DOI:10.1021/la5009335).
45 A. Goyal, C. K. Hall and O. D. Velev, *Soft Matter,* 2010, **6**, 480-484 (DOI:10.1039/b907873h).
46 P. A. Monson and M. Rigby, *Mol. Phys.,* 1980, **39**, 977-988 (DOI:10.1080/00268978000100831).
47 M. Adams, Z. Dogic, S. L. Keller and S. Fraden, *Nature,* 1998, **393**, 349-352 (DOI:10.1038/30700).
48 F. Brochard and P. Gennes, *Journal De Physique,* 1970, **31**, 691-& (DOI:10.1051/jphys:01970003107069100).
49 A. Mertelj, D. Lisjak, M. Drofenik and M. Copic, *Nature,* 2013, **504**, 237-+ (DOI:10.1038/nature12863).
50 S. D. Peroukidis and S. H. L. Klapp, *Phys Rev E.,* 2015, **92**, 010501 (DOI:10.1103/PhysRevE.92.010501).
51 S. D. Peroukidis, K. Lichtner and S. H. L. Klapp, *Soft Matter,* 2015, **11**, 5999-6008 (DOI:10.1039/c5sm00903k).
52 S. D. Peroukidis and S. H. L. Klapp, *Soft Matter,* 2016, **12**, 6841-6850 (DOI:10.1039/c6sm01264g).
53 M. A. Bates and D. Frenkel, *J. Chem. Phys.,* 2000, **112**, 10034-10041 (DOI:10.1063/1.481637).
54 W. Wu and J. B. Tracy, *Chemistry of Materials,* 2015, **27**, 2888-2894 (DOI:10.1021/cm504764v).
55 A. Bellemans, J. Orban and D. Vanbelle, *Mol. Phys.,* 1980, **39**, 781-782 (DOI:10.1080/00268978000100671).
56 D. C. Rapaport, *J. Chem. Phys.,* 1979, **71**, 3299-3303 (DOI:10.1063/1.438770).
57 J. S. Rowlinson, *Physica A-Statistical Mechanics and its Applications,* 1989, **156**, 15-34 (DOI:10.1016/0378-4371(89)90108-8).
58 K. A. Kozek, K. M. Kozek, W. Wu, S. R. Mishra and J. B. Tracy, *Chemistry of Materials,* 2013, **25**, 4537-4544 (DOI:10.1021/cm402277y).
59 H. C. Andersen, *J. Chem. Phys.,* 1980, **72**, 2384-2393 (DOI:10.1063/1.439486).
60 H. Neitsch and S. H. L. Klapp, *J. Chem. Phys.,* 2013, **138**, 064904 (DOI:10.1063/1.4790406).
61 S. K. Smoukov, S. Gangwal, M. Marquez and O. D. Velev, *Soft Matter,* 2009, **5**, 1285-1292 (DOI:10.1039/b814304h).

We calculate phase diagrams for dipolar rod and disc mixtures and compare mixture phases to those of single component systems.